Bio-silica incorporated barium ferrite composites: Evaluation of structure, morphology, magnetic and microwave absorption traits

by Wahyu Widanarto

Submission date: 06-Oct-2019 07:49PM (UTC+0700)
Submission ID: 1186899221
File name: Manuscript_SiBF-corrected_turnitin.docx (627.49K)
Word count: 3281
Character count: 18733

Bio-silica incorporated barium ferrite composites: Evaluation of structure, morphology, magnetic and microwave absorption traits

ABSTRACT

Wireless communications and electronic devices based on microwave (MW) frequency are useful due to several implications. In this view, a series of bio-silica ion incorporated barium-ferrite-composites with the composition of (x)Bio-SiO_2:(80-x)Fe_2O_3:(20)BaO, where x = 0, 1, 2, and 3 wt% was prepared using the modified solid-state reaction. The impact of different bio-silica (extricated from sintered rice husk) substances on the surface morphologies, structures, and magnetic characteristics of these composites were assessed. The relative complex permittivity and permeability were resolved using the Nicholson-Ross-Weir strategy in the frequency range of 8–13 GHz. Meanwhile, the reflection loss was considered through the Transmission/reflection line theory to assess the MW absorption properties of the composites. Incorporation of bio-silica in barium ferrite composites generated a new hexagonal phase of $Ba_3Fe_{32}O_{51}$, and a tetragonal phase of $BaFeSi_4O_{10}$ lead to decreasing in the saturation magnetization and significant shifting in peaks of MW frequency absorption.

Keywords: bio-silica, barium ferrite, magnetic properties, permittivity, permeability, reflection loss

1. Introduction

In recent times, microwave (MW) absorbing materials became one of the key high-tech candidates for the development of the high-performance device in the field of anti-radar technology, wireless communications, and shielding of electromagnetic wave interferences [1–3]. The coating of the targets with MW absorbing materials emerged as a strategy to reduce the intensity of the reflected electromagnetic waves. This technique utilizes the absorption or dispersion of electromagnetic energy in the material medium between the electromagnetic wave source and the protected target. For such purposes, materials must be fit for weakening and dispersing the overabundance measure of the electromagnetic radiation in the form of heat through the mechanisms of magnetic and dielectric loss [4]. Likewise, innovative magnetic materials particularly ferrites based, are uncovered to be suitable for absorbing the MW and have frequently been investigated [5–13].

It has been verified that a barium ferrite system (a magnetic material) with a wide crystalline anisotropic magnetic field can potentially be used in the GHz frequency range compared to other ferrites with spinel and garnet structures [2,14]. Thus, the barium-hexaferrites (BHFs) owing to their amazingly strong uniaxial anisotropic magnetic field were prepared as MW absorbing

material [6–8,15,16]. The literature revealed that the replacement of Fe^{3+} by trivalent lanthanide ions (used as doping agent) is an effective way to shift the resonant frequency (f_r) and change the anisotropy field (H_A), influencing the MW absorption capacity of the magnetic material [2,9,17–21]. However, the scarcity and high prices of rare earth materials limit their widespread usages. Thus, the exploration of the doping agent alternative to the rare-earth ions (acts as an activator) became mandatory to fulfill such need.

Categorically, silica is a famous semiconducting material that can be obtained either commercially or from plentiful natural resources. Interestingly, rice husk after complete combustion can be a great source of bio-silica [16,17]. Such bio-silica derived from rice husk (as abundant raw material) has several advantages compared to silica minerals, including the existence of fine grain, high reactivity, low cost and can function as a heavy metal binder. Encouraged by these notable benefits of rice husk extracted bio-silica, we prepared some bio-silica integrated barium ferrite composites (hereafter called SiBFCs) to reduce the values of coercive field (H_c) and saturation magnetization (M_s), in that way enhancement of the selective MW absorption capacity of the achieved SiBFCs.

This paper reports the synthesis and characterizations of the newly prepared SiBFCs, wherein the bio-silica at various concentrations were merged in pure barium hexaferrites (BHFs). The undoped and doped composites were synthesized via solid–state reactions. These as-prepared SiBFCs were characterized using diverse analytical apparatuses to assess the impact of varying Si^{4+} doping levels on the microstructure, morphology, magnetic properties, and MW reflection losses in the frequency range of GHz. The obtained $BaFeSi_4O_{10}$ and $Ba_3Fe_{32}O_{51}$ composites were given away to be valuable for several applications.

2. Experimental Procedures

Four samples of SiBFCs with the composition of (x)Bio-SiO_2:$(80\text{-}x)Fe_2O_3$:(20)BaO, (x = 0, 1, 2 and 3 in wt%) were synthesized via the modified solid-state reaction. Highly pure powders of $BaCO_3$ (from Merck with purity of 99%), bio-silica, and γ-Fe_2O_3 as primary raw constituents to prepare these SiBFCs. The $BaCO_3$ powder was calcined at 350 °C for 15 minutes to eliminate the presence of the carbon component. The bio-silica was obtained by sintering the rice husk ash in the furnace at a temperature of 1000 °C for three hours. Meanwhile, Fe_3O_4 was extracted from iron sand [22] and sintered at 850 °C for three hours to obtain γ-Fe_2O_3. Afterward, We mixed bio-

silica powder gradually with γ-Fe_2O_3 and BaO powder. The mixed constituent powder was compressed to yield the pellet of 1 mm thick and 1 cm diameter [19]. Additionally, all the pellets were strengthened and sintered at 800 °C (for one hour) and 1100 °C (for 5 hours) before they were cooled down to the room temperature naturally. The acquired pellets were named as SiBF0, SiBF1, SiBF2, and SiBF3, depending on the matching bio-silica content of 0, 1, 2, and 3 wt%. For further characterizations, we crushed and glued some pellets with resin to get a rectangular-shaped sample of dimension (2.3 cm × 1.0 cm × 0.5 cm) using a WR90 sample holder.

The surface morphology and microstructure of the synthesized SiBFCs were characterized using the scanning electron microscope (SEM, Hitachi SU 3500) [19,21,23]. The crystalline nature of the prepared SiBFCs were confirmed using the X-ray diffraction (XRD, SmartLab 3 kW) furnished with Cu–Kα radiation of wavelength (λ) ≈ 0.1541874 nm. The vibrating sample magnetometer (VSM, Oxford 1.2H) was used to scrutinize the magnetic traits of the proposed samples. The scattering parameters (*S*) of the samples were recorded on a vector network analyzer (VNA, Keysight PNA-L N5232A) operated in the frequency range of 8–13 GHz. The MW absorption measurement was conducted to yield the scattering parameters such as S_{11}, S_{12}, S_{21}, and S_{22} (*S*-parameters). The value of S_{11} (= S_{22}) signified the reflection coefficient (Γ) and S_{21} (= S_{12}) represented the transmission coefficient (*T*). The values of relative complex permeability (μ_r) and permittivity (ε_r) were obtained following the Nicholson-Ross-Weir (NRW) relations given by:

$$\mu_r = \frac{1+\Gamma}{\Lambda(1-\Gamma)\sqrt{\frac{1}{\lambda_0^2}-\frac{1}{\lambda_c^2}}} \tag{1}$$

$$\frac{1}{\Lambda^2} = -\left[\frac{1}{2\pi d}\ln\left(\frac{1}{T}\right)\right]^2 \tag{2}$$

$$\varepsilon_r = \frac{\lambda_0^2}{\mu_r}\left(\frac{1}{\lambda_c^2}-\left[\frac{1}{2\pi d}\ln\left(\frac{1}{T}\right)\right]^2\right) \tag{3}$$

where λ_0 is the wavelength in vacuum, λ_c is the cut-off wavelength, *c* is the speed of the light, and d is the thickness of the sample.

3. Results and Discussions

3.1. Structures and Phases

Fig. 1 depicts the XRD pattern of the synthesized bio-silica. It confirms that all diffraction peaks are attributed to SiO_2 with a tetragonal crystal system. Fig. 2 displays the XRD diffractograms of the produced SiBFCs that consisted of many characteristic peaks assigned to altering crystalline lattices. All the observed peaks in the pristine sample (SiBF0 without bio-silica incorporation) were due to the main hexagonal crystalline lattice of $BaFe_{12}O_{19}$ and tallied to the ICDD card number 00-039-1433 with crystal configurations of $a = b = 0.5894$ nm, $c = 2.3215$ nm, $\alpha = \beta = 90°$ and $\gamma = 120°$. Nevertheless, the appeared peak at 27.52° was due to the monoclinic crystalline phase of $Ba_2Fe_2O_5$ that corresponded to the ICDD card number 00-043-0256. The XRD pattern of SiBF1 sample revealed that the replacement of Fe^{3+} in the barium ferrite lattice by Si^{4+} ions at 1 wt% of SiO_2 did not cause any significant changes of the crystal structures. The appearance of two dominant peaks in SiBF1 confirmed the formation of the major phase of $Ba_3Fe_{32}O_{51}$ and minor phase of barium iron silicate $BaFeSi_4O_{10}$. The occurrences of sharp XRD peaks were due to the hexagonal crystal lattice of $Ba_3Fe_{32}O_{51}$ that corresponded to the ICDD card number 00-041-0846 with the crystal configurations of $a = b = 0.5892$ nm, $c = 2.3198$ nm, $\alpha = \beta = 90°$ and $\gamma = 120°$. Moreover, the peaks centered at 26.52° and 35.48° were assigned to the tetragonal crystal lattice planer orientation of $BaFeSi_4O_{10}$ (tallied to the ICDD card number 00-003-0402). The XRD pattern of the composite prepared with two wt% of bio-silica revealed a new phase of barium silicate $Ba_3Si_5O_{13}$ with a monoclinic crystalline lattice structure (agreed to the ICDD number 00-026-0179). The composite containing three wt% of bio-silica exhibited the dominant barium iron silicate $BaFeSi_4O_{10}$ ordered phase. It was claimed that the replacement of Fe^{3+} ions by Si^{4+} in the produced BFCs can create another significant hexagonal phase of $Ba_3Fe_{32}O_{51}$ and a tetragonal phase of $BaFeSi_4O_{10}$. The observed broadening in the XRD peaks for all the studied SiBFCs is attributed to the insolvent of lattice strain and nano-crystallites size confinement effects [24,25].

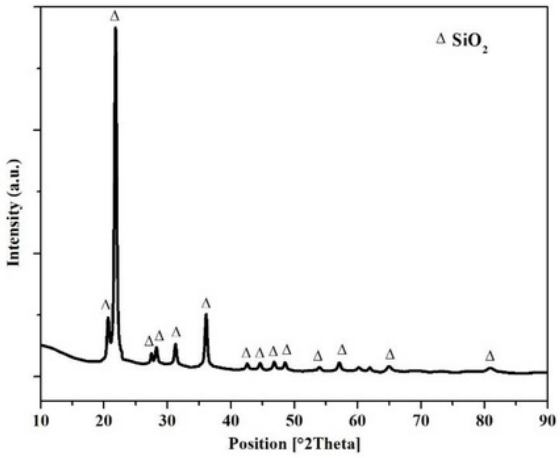

Fig. 1. The XRD pattern of the bio-silica (SiO_2) at 1000 °C

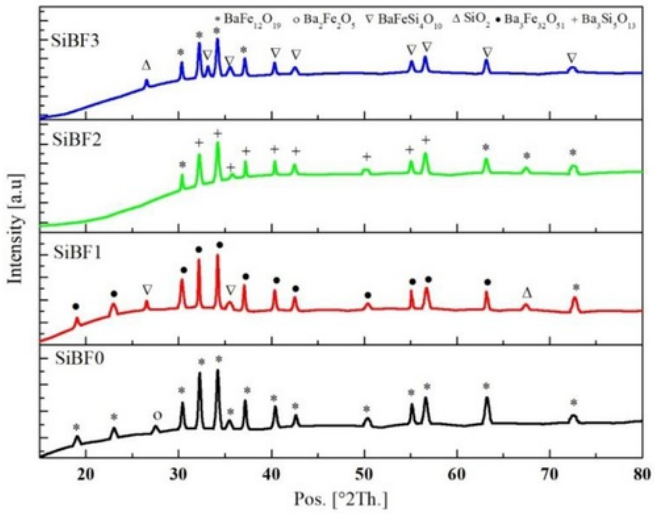

Fig. 2. The XRD patterns of the Si^{4+} undoped and doped SiBFCs

3.2. Surface morphology

Fig. 3 shows the SEM micrographs of the prepared SiBFCs. The surface morphologies of the composites consisted of rough microstructures with high porosity. The composite particles within the samples were bonded tightly to each other and formed some intergranular pores due to the occupation Si^{4+} ions in the preferred lattice sites. Consequently, more porous microstructures

are formed on the surface. These pores, in turn, can favor the entrapment of the MW and its subsequent scattering in all directions by the surface of the particle present in the pores. In all the synthesized SiBFCs, these particles disclose a typical hexagonal morphology with the particle size of about 0.5 μm

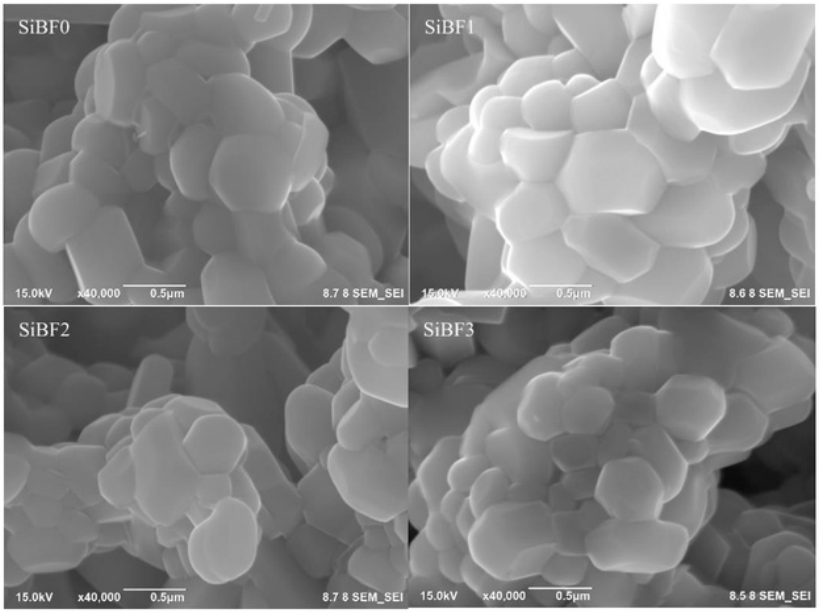

Fig. 3. The SEM images of the SiBFCs

Fig. 4 represents the room temperature hysteresis loops (*M-H* curves) of the as-synthesized SiBFCs. The values of saturation magnetization of the studied SiBFCs are decreased (from 39.5 to 30.4 emu/g) significantly with the addition of bio-silica (from 1 to 3 wt%) into the composites. However, the coercive field values (altered from 775.9 – 811.0 Oe) are not affected appreciably due to the increase in bio-silica contents. The maximum reduction in the saturation magnetization displayed by the SiBF3 sample is ascribed to the presence of dominant tetragonal barium iron silicate ($BaFeSi_4O_{10}$) crystalline phase in the composite. The coercive field values of the composites are observed to increase slightly due to the rise in bio-silica contents. With the increase in bio-silica content from 0 to 2 wt%, the area of the hysteresis loop of the SiBFCs enlarges from 15.9 to 31.0 kOe.emu/g, respectively. Furthermore, the hysteresis loop area of SiBFC shrinks at three wt% of bio-silica. The observed change in the magnetic permeability of SiBFCs with the addition of bio-silica into the composites is majorly attributed to the alteration in the saturation magnetization and coercive field values.

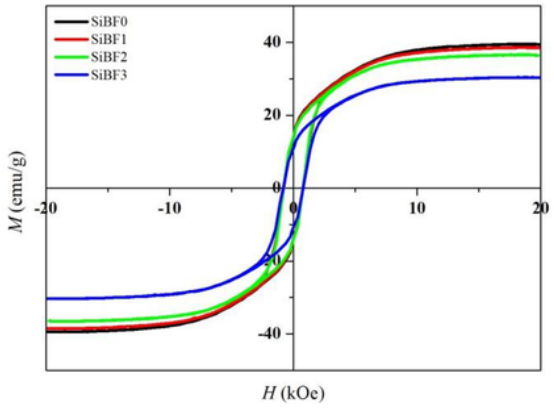

Fig. 4. The room temperature *M-H* loops of the SiBFCs

Fig. 5(a) describes the frequency dependence of the relative permeability ($\mu_r = \mu' + \mu''$) of all the SiBFCs. The real part of the permeability (μ') specifies a gradual decrease in their magnetic energy storing capacity due to polarization of magnetic dipole in higher MW frequency. The μ' value of the composites drops from about 2.5 (for SiBF0 and SiBF2) and 0.9 (for SiBF1 and SiBF3) to near-zero with the increase in bio-silica content from 0 to 3 wt%. Meanwhile, the observed magnetic loss is revealed by the imaginary part of the permeability (μ''). The μ'' value of SiBF0 and SiBF2 declines rapidly from 0.9 to near 0 and almost remains constant near zero for SiBF1 and SiBF3 due to the relaxation process, which generates dissipation energy of MV as thermal energy.

Fig. 5(b) displays the frequency-dependent relative complex permittivity ($\varepsilon_r = \varepsilon' + \varepsilon''$) of all SiBFCs, where ε' and ε'' are the real and imaginary part of the permittivity, respectively. The value of ε' indicated the lack of energy absorption by the composite from an externally applied electric field [26]. The values of ε' for the composite without bio-silica doping (SiBF0) were dropped sharply. Conversely, the values of ε' for composites containing bio-silica (1 to 3 wt%) were increased significantly above 12 GHz due to the electrical dipole polarization. The values of ε'' (called the loss factor) denotes the electrical energy dissipation ability of the SiBFCs. The values of ε'' for all SiBFCs were decreased gradually with the rise in the frequency.

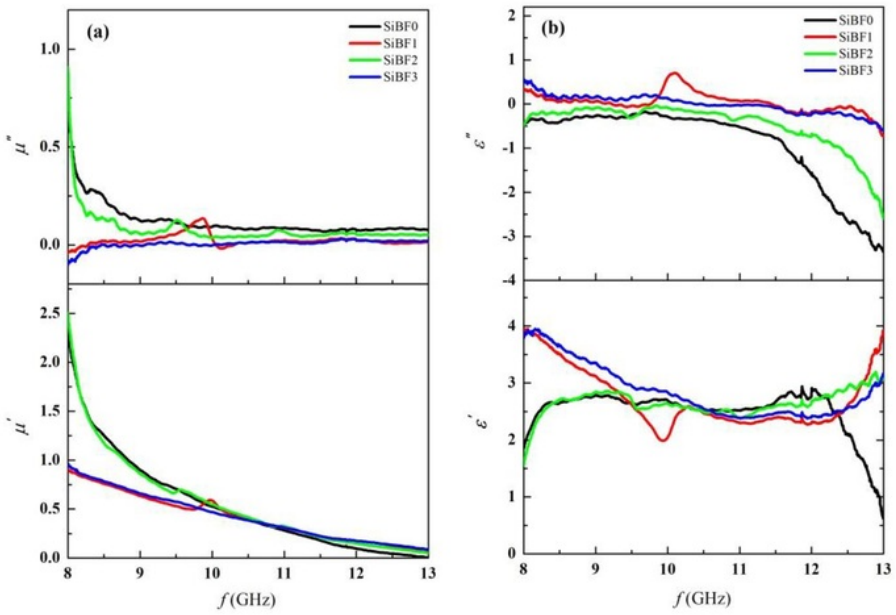

Fig. 5. Frequency dependent (a) permeability and (b) permittivity of the SiBFCs

The MW absorption properties of SiBFCs were evaluated by calculating the values of reflection loss (R_L) based on the transmission/reflection line theory [6, 27–29]:

$$R_L = -20\log\left|\frac{Z_{in} - Z_0}{Z_{in} + Z_0}\right| \quad (4)$$

$$Z_{in} = Z_0\sqrt{\frac{\mu_r}{\varepsilon_r}}\tanh\left[j\frac{2\pi f d}{c}\sqrt{\mu_r\varepsilon_r}\right] \quad (5)$$

where Z_0 and Z_{in} are the corresponding intrinsic impedance in vacuum and the input impedance in the material, f represents the MW frequency, d denotes the sample thickness, and c is the light speed in the vacuum.

Fig. 6 illustrates the frequency dependent changes in the values of R_L of the prepared SiBFCs. The value of R_L for SiBF0 was value less than -10 dB at the frequency of 8.35, 9.37, and 10.60 GHz. The band positions (peak frequencies) of the composites disclose a significant shift with the change in bio-silica contents with the bandwidth of less than 1 GHz. The sample prepared with one wt% of bio-silica (SiBF1) reveals the lowest R_L value of -28.56 dB at the frequency of 12.18 GHz. This disclosure affirms that the MW absorption capacity of the proposed SiBFCs can

be essentially customized by controlling the impurity or dopant (bio-silica) concentration, fulfilling the application demand at various frequencies.

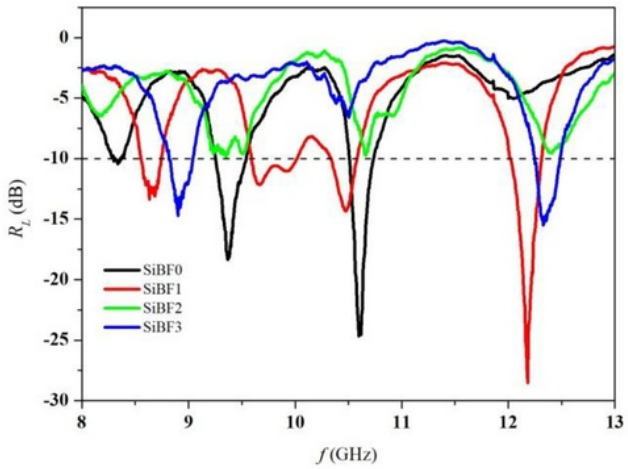

Fig. 6. Reflection loss of the SiBFCs as a function of MW frequency

4. Conclusions

Considering the MW absorption potency of barium ferrites and its usefulness in wireless communications, we synthesized four samples of SiBFCs (without and with bio-silica activation) via the modified solid-state reaction approach. Rice husk derived abundant and cheap bio-silica was doped into the barium ferrites to improve their magnetic and MW absorption attributes. The structure of the studied composites revealed the presence of various crystalline phases. The surface of SiBFCs disclosed hexagonal morphology with a particle size of about 0.5 μm. The surface morphology, structure, MW reflection loss, permittivity, permeability, coercivity, saturation magnetization, and MW absorption of the proposed SiBFCs were found to be sensitive to the substitution of Fe^{3+} by Si^{4+} ions into the composite matrix. It was established that the MW absorption ability of the newly composed SiBFCs can be tailored by adjusting the bio-silica content. Present knowledge may contribute towards the development of SiBFCs based MW absorption devices.

Acknowledgments

The authors appreciated the financial support from the Universitas Jenderal Soedirman, Kemenristekdikti Indonesia, and UTM Malaysia (MOHE, FRGS/KPT 5F050).

References

[1] H. Zhao, G. Zhang, R. MA, Synthesis and electromagnetic properties of nanocrystalline Ni-Zn Ferrite doped lanthanum, Nanotechnol. Precis. Eng. 8 (2010).

[2] C.-J. Li, B. Wang, J.-N. Wang, Magnetic and Microwave Absorbing Properties of Electrospun Ba(1−x)LaxFe12O19 Nanofibers, J. Magn. Magn. Mater. 324 (2012) 1305–1311. doi:10.1016/j.jmmm.2011.11.016.

[3] B.K. Rai, S.R. Mishra, V.V. Nguyen, J.P. Liu, Synthesis and characterization of high coercivity rare-earth ion doped Sr0.9RE0.1Fe10Al2O19 (RE: Y, La, Ce, Pr, Nd, Sm, and Gd), J. Alloys Compd. 550 (2013) 198–203. doi:10.1016/j.jallcom.2012.09.021.

[4] M.S. Kim, J.G. Koh, Microwave-absorbing characteristics of NiCoZn ferrite prepared by using a co-precipitation method, J. Korean Phys. Soc. 53 (2008) 737–741.

[5] C.L. Yuan, Y.S. Tuo, Microwave adsorption of Sr(MnTi)xFe12−2xO19 particles, J. Magn. Magn. Mater. 342 (2013) 47–53. doi:10.1016/j.jmmm.2013.04.038.

[6] C. Sun, K. Sun, P. Chui, Microwave absorption properties of Ce-substituted M-type barium ferrite, J. Magn. Magn. Mater. 324 (2012) 802–805. doi:10.1016/j.jmmm.2011.09.023.

[7] C. Dong, X. Wang, P. Zhou, T. Liu, J. Xie, L. Deng, Microwave magnetic and absorption properties of M-type ferrite BaCoxTixFe12−2xO19 in the Ka band, J. Magn. Magn. Mater. 354 (2014) 340–344. doi:10.1016/j.jmmm.2013.11.008.

[8] S. Salman, S.S.S. Afghahi, M. Jafarian, Y. Atassi, Microstructural and magnetic studies on BaMgxZnxX2xFe12−4xO19 (X=Zr,Ce,Sn) prepared via mechanical activation method to act as a microwave absorber in X-band, J. Magn. Magn. Mater. 406 (2016) 184–191. doi:10.1016/j.jmmm.2016.01.020.

[9] Z. Qiao, S. Pan, J. Xiong, L. Cheng, Q. Yao, P. Lin, Magnetic and microwave absorption properties of La-Nd-Fe alloys, J. Magn. Magn. Mater. 423 (2017) 197–202. doi:10.1016/j.jmmm.2016.08.093.

[10] R. Taurino, A. Karamanov, R. Rosa, E. Karamanova, L. Barbieri, S. Atanasova-Vladimirova, G. Avdeev, C. Leonelli, New ceramic materials from MSWI bottom ash obtained by an innovative microwave-assisted sintering process, J. Eur. Ceram. Soc. 37 (2017) 323–331. doi:10.1016/j.jeurceramsoc.2016.08.011.

[11] G. Liu, L. Wang, Z. Yang, R. Wu, Synthesis of iron-based hexagonal microflakes for strong microwave attenuation, J. Alloys Compd. 718 (2017) 46–52. doi:10.1016/j.jallcom.2017.05.100.

[12] M. Bibi, S.M. Abbas, N. Ahmad, B. Muhammad, Z. Iqbal, U.A. Rana, S.U.D. Khan, Microwaves absorbing characteristics of metal ferrite/multiwall carbon nanotubes nanocomposites in X-band, Compos. Part B Eng. 114 (2017) 139–148. doi:10.1016/j.compositesb.2017.01.034.

[13] J. Luo, S. Pan, L. Cheng, P. Lin, Y. He, J. Chang, Electromagnetic and microwave absorption properties of Er-Ho-Fe alloys Jialiang, J. Rare Earths. 36 (2018) 715–720.

doi:10.1016/j.jre.2018.02.006.

[14] W. Li, X. Qiao, M. Li, T. Liu, H.X. Peng, La and Co substituted M-type barium ferrites processed by sol-gel combustion synthesis, Mater. Res. Bull. 48 (2013) 4449–4453. doi:10.1016/j.materresbull.2013.07.044.

[15] Y. Liu, T.J. Wang, Y. Liu, X.J. Li, Y. Liu, Mechanism for Synthesizing Barium Hexagonal Ferrite by Sol-Gel Method, Adv. Mater. Res. 549 (2012) 105–108. doi:10.4028/www.scientific.net/AMR.549.105.

[16] S. Bierlich, F. Gellersen, A. Jacob, J. Töpfer, Low-temperature sintering and magnetic properties of Sc- and In-substituted M-type hexagonal barium ferrites for microwave applications, Mater. Res. Bull. 86 (2017) 19–23. doi:10.1016/j.materresbull.2016.09.025.

[17] W. Jing, Z. Hong, B. Shuxin, C. Ke, Z. Changrui, Microwave absorbing properties of rare-earth elements substituted W-type barium ferrite, J. Magn. Magn. Mater. 312 (2007) 310–313. doi:10.1016/j.jmmm.2006.10.612.

[18] G. Shen, Z. Xu, Y. Li, Absorbing properties and structural design of microwave absorbers based on W-type La-doped ferrite and carbon fiber composites, J. Magn. Magn. Mater. 301 (2006) 325–330. doi:10.1016/j.jmmm.2005.07.007.

[19] W. Widanarto, F. Amirudin, S.K. Ghoshal, M. Effendi, W.T. Cahyanto, Structural and magnetic properties of La3+ substituted barium−natural nanoferrites as microwave absorber in X-band, J. Magn. Magn. Mater. 426 (2017) 483–486. doi:10.1016/j.jmmm.2016.11.124.

[20] L. Deng, L. Ding, K. Zhou, S. Huang, Z. Hu, B. Yang, Electromagnetic properties and microwave absorption of W-type hexagonal ferrites doped with La3+, J. Magn. Magn. Mater. 323 (2011) 1895–1898. doi:10.1016/j.jmmm.2011.02.034.

[21] W. Widanarto, E. Ardenti, S.K. Ghoshal, C. Kurniawan, M. Effendi, W.T. Cahyanto, Significant reduction of saturation magnetization and microwave-reflection loss in barium-natural ferrite via Nd3+ substitution, J. Magn. Magn. Mater. 456 (2018) 288–291. doi:10.1016/j.jmmm.2018.02.050.

[22] W. Widanarto, M. Jandra, S.K. Ghoshal, M. Effendi, W.T. Cahyanto, BaCO3 mediated modifications in structural and magnetic properties of natural nanoferrites, J. Phys. Chem. Solids. 79 (2015) 78–81. doi:10.1016/j.jpcs.2014.12.011.

[23] W. Widanarto, F.M. Rahayu, S.K. Ghoshal, M. Effendi, W.T. Cahyanto, Impact of ZnO substitution on magnetic response and microwave absorption capability of strontium-natural nanoferrites, Results Phys. 5 (2015) 253–256. doi:10.1016/j.rinp.2015.09.002.

[24] V.S. Vinila, R. Jacob, A. Mony, H.G. Nair, S. Issac, S. Rajan, A.S. Nair, J. Isac, XRD Studies on Nano Crystalline Ceramic Superconductor PbSrCaCuO at Different Treating Temperatures, Cryst. Struct. Theory Appl. 03 (2014) 1–9. doi:10.4236/csta.2014.31001.

[25] S. Dabagh, A.A. Ati, R.M. Rosnan, S. Zare, Z. Othaman, Effect of Cu – Al substitution on the structural and magnetic properties of Co ferrites, Mater. Sci. Semicond. Process. 33 (2015) 1–8. doi:10.1016/j.mssp.2015.01.025.

[26] C.K. Das, P. Bhattacharya, S.S. Kalra, Graphene and MWCNT: Potential Candidate for Microwave Absorbing Materials, J. Mater. Sci. Res. 1 (2012) p126. doi:10.5539/jmsr.v1n2p126.

[27] K. Shi, J. Li, S. He, H. Bai, Y. Hong, Y. Wu, D. Jia, Z. Zhou, A superior microwave absorption

material: Ni 2+ -Zr 4+ Co-Doped barium ferrite ceramics with large reflection loss and broad bandwidth, Curr. Appl. Phys. 19 (2019) 842–848. doi:10.1016/j.cap.2019.03.018.

[28] P. Meng, K. Xiong, L. Wang, S. Li, Y. Cheng, G. Xu, Tunable complex permeability and enhanced microwave absorption properties of BaNixCo1-xTiFe10O19, J. Alloys Compd. 628 (2015) 75–80. doi:10.1016/j.jallcom.2014.10.163.

[29] S. Kumar, R. Chatterjee, Complex permittivity , permeability , magnetic and microwave absorbing properties of Bi 3+ substituted U-type hexaferrite, J. Magn. Magn. Mater. 448 (2018) 88–93. doi:10.1016/j.jmmm.2017.06.123.

Bio-silica incorporated barium ferrite composites: Evaluation of structure, morphology, magnetic and microwave absorption traits

ORIGINALITY REPORT

11%	1%	9%	10%
SIMILARITY INDEX	INTERNET SOURCES	PUBLICATIONS	STUDENT PAPERS

PRIMARY SOURCES

1	Wahyu Widanarto, Siti Khaeriyah, Sib Krishna Ghoshal, Candra Kurniawan, Mukhtar Effendi, Wahyu Tri Cahyanto. "Selective microwave absorption in Nd3+ substituted barium ferrite composites", Journal of Rare Earths, 2019 Publication	4%
2	Submitted to Universitas Jenderal Soedirman Student Paper	4%
3	W. Widanarto, F. Amirudin, S.K. Ghoshal, M. Effendi, W.T. Cahyanto. "Structural and magnetic properties of La 3+ substituted barium−natural nanoferrites as microwave absorber in X-band", Journal of Magnetism and Magnetic Materials, 2017 Publication	2%
4	Submitted to Indian Institute of Science, Bangalore Student Paper	1%

Exclude quotes	On	Exclude matches	< 1%
Exclude bibliography	On		